IEEE Access
Multidisciplinary ⋮ Rapid Review ⋮ Open Access Journal

Received 3 April 2023, accepted 14 April 2023, date of publication 18 April 2023, date of current version 25 April 2023.

Digital Object Identifier 10.1109/ACCESS.2023.3268116

METHODS

A Low-Cost System for Far-Field Non-Anechoic Measurements of Antenna Performance Figures

JAN OLENCKI[1], VORYA WALADI[1], ADRIAN BEKASIEWICZ[1], (Senior Member, IEEE), AND LEIFUR LEIFSSON[2]

[1]Faculty of Electronics, Telecommunications and Informatics, Gdańsk University of Technology, 80-233 Gdańsk, Poland
[2]School of Aeronautics and Astronautics, Purdue University, West Lafayette, IN 47907, USA

Corresponding author: Adrian Bekasiewicz (bekasiewicz@ru.is)

This work was supported in part by the National Science Center of Poland under Grant 2021/43/B/ST7/01856, and in part by the National Center for Research and Development under Grant NOR/POLNOR/HAPADS/0049/2019-00.

ABSTRACT Prototype measurements are the key step in the development of antenna structures. Typically, their far-field characteristics are validated in expensive, dedicated facilities such as open range sites, or anechoic chambers. Despite being necessary for obtaining high-precision data (e.g., for device qualification), the use of costly infrastructure might not be fully justified when the main goal of measurements includes demonstration of the methodology behind determination of the performance figures of interest (e.g., for the purpose of teaching), or rough validation of the EM simulation model correctness. From this perspective, systems for far-field measurements in non-anechoic environments represent an interesting alternative to the utilization of the state-of-the-art equipment and facilities. Despite their proven usefulness, the mentioned systems are normally constructed around the expensive, laboratory-grade equipment, which contradicts the whole concept of low-cost measurements. This paper discusses a cost-efficient, mobile system for experimental validation of antennas. Its main components include the in-house developed rotary heads, an open-hardware-based vector network analyzer, and the measurements post-processing software. The cost of the system amounts to only around 3630 USD. The capabilities of the device have been demonstrated through measurements of two antenna structures. The considered performance figures include radiation pattern and single-direction gain vs. frequency. Comparisons against the measurements performed in benchmark conditions (anechoic chamber), as well as using professional network analyzer have also been provided. Furthermore, the documentation that facilitates the construction of the system components is shared in an online repository.

INDEX TERMS Antenna measurements, compact radiators, gain, internet things, non-anechoic measurements, time-gating method, radiation patterns.

I. INTRODUCTION

Measurement of the fabricated prototype is one of the key steps in the development of microwave/antenna components. The main goal of the process is to ensure that the electromagnetic (EM) simulation models utilized in the course of structure design satisfy the prescribed performance requirements. For the considered classes of components, the electrical properties are normally expressed in the form of a scattering matrix which can be obtained using a vector network analyzer (VNA). Microwave circuits such as filters or couplers, are normally characterized using performance figures such as insertion/return loss, or transmission, which are contained in the S-parameter matrix. Nevertheless, the performance of antenna structures is represented using both electrical (i.e., return loss) and field-related (i.e., radiation patterns, gain, and/or axial ratio) characteristics [1], [2]. The latter ones are obtained indirectly through the post-processing of multiple S-parameter matrices. A typical setup for far-field measurements includes the antenna under test (AUT), the reference

The associate editor coordinating the review of this manuscript and approving it for publication was Hassan Tariq Chattha.

antenna (RA)—both mounted on the dedicated rotary heads that determine angular positions between the radiators—and the VNA. From the VNA perspective, the RA-AUT system is a two-port device where S-matrix-based transmission is realized through a wireless medium. Hence, the far-field properties of the AUT can be extracted based on the analysis of transmission changes as a function of e.g., its angular position.

As already mentioned, the RA-AUT transmission is realized through a wireless medium, the conditions of which substantially affect the measurement performance. This, so-called, dynamics of the propagation environment is understood as variations of its physical properties as a function of time. The latter ones are affected (among others) by factors such as air humidity, or temperature (as well as their gradients), but also by EM noise that stems from interferences due to multi-path transmission of RA-AUT signals, but also from the presence of the external EM sources (e.g., microwave systems that operate in the vicinity of the test setup) [3], [4], [5]. To minimize the effects of environment on the quality of measurements, antenna prototypes are normally characterized at dedicated test sites that maintain strict control of the propagation conditions. Appropriate conditions can be obtained in anechoic chambers, which provide enclosure for the measurement system (a Faraday cage) in order to isolate of the test site from the external EM signal sources. Furthermore, the chambers are lined with materials that ensure absorption of RA-AUT signals that would normally contribute to multi-path interferences (e.g., due to reflections from walls) [5], [6], [7], [8], [9]. Alternatively, antenna performance can be characterized at outdoor test sites located in remote, unpopulated, and flat areas. Such environments are free from artificial EM radiation sources and mitigate multi-path fading due to lack of objects from which the RA-AUT signals could be reflected [5], [7], [8], [9], [10], [11]. Despite their usefulness for accurate characterization of antenna performance, the strict requirements and conditions offered by the mentioned test sites make their construction an overly expensive enterprise. Regardless of maintaining a desirable radiation environment, the discussed facilities require laboratory-grade measurement equipment in the form of signal sources, detectors, amplifiers and the necessary connectivity gear that further contributes to the cost of their development [3], [4], [5].

The use of professional test sites and equipment may not be justified for applications such as education, where explanation of the procedures behind measurement of antenna properties is more important than obtaining high fidelity of the results. Furthermore, avoiding the use of expensive equipment and the need for dedicated test sites would substantially reduce the cost of the system. With that in mind, any possible damage to the equipment resulting from misuse (e.g., by students, or insufficiently trained personnel) would not be associated with overwhelmingly high repair costs. From this perspective, the availability of cheap, yet reliable systems for the characterization of antenna far-field properties seems to be of interest for applications characterized by a highly constrained budget, and/or moderate requirements in terms of measurement precision.

Non-anechoic test sites represent a cost-efficient alternative to the validation of antenna performance in strictly controlled environments [7], [8], [12]. Their construction is limited to the installation of positioning towers along with the signal source and detector (typically in the form of a VNA) while neglecting either all, or selected (i.e., the most expensive) components of the test site that are dedicated to maintaining control over the propagation environment [12], [13]. In other words, non-anechoic measurements can be performed in locations that are not tailored (in terms of propagation conditions) to far-field experiments such as office rooms, hallways, or courtyards. Alternatively, the tests can be realized in partially controlled environments in the form of e.g., reverberation chambers which isolate the external EM interferences [4]. Unfortunately, the measurements performed in the discussed conditions are subject to substantial EM interferences. Consequently, they are useless for drawing conclusions about the AUT's performance unless additional post-processing of the obtained data is performed. It is worth noting that, although not mandatory, after-treatment of RA-AUT transmission measured in dedicated test-sites can also improve the responses fidelity [9], [10], [11], [12], [13].

The refinement methods for non-anechoic, far-field antenna measurements fall into two main categories: (i) extraction of the AUT performance based on its measurements over a selected bandwidth around the frequency of interest [7], [8], [9], [12], [13], [14], [15], [16], [17], [18] and (ii) characterization of the propagation environment based on comparative analysis of the AUT performance [16], [17], [18]. In essence, both groups of techniques focus on the determination of the AUT responses for line-of-sight (LoS) propagation while removing the interferences resulting from non-LoS transmission and other EM noise. In [19], a time-domain representation of the RA-AUT response is modified using the gating window centered around the fraction of the impulse response corresponding to LoS transmission. The resulting signal is converted back to the frequency spectrum. The post-processing is performed for each angular position of the RA-AUT system in order to extract the radiation characteristics of the antenna. The discussed time-gating method (TGM) proved to be useful for correcting the measurements in a variety of environments including open-test sites, as well as anechoic and reverberation chambers [7], [12], [14]. The Matrix-pencil method is another multi-frequency correction technique [18]. It is oriented towards approximation of transmission between the measured antennas using a series of functions that correspond to the LoS and reflected signals [19], [20]. Their coefficients are then used in order to reconstruct the LoS transmission while neglecting interferences [18], [19], [20]. An alternative approach involves the representation of transmission

responses using Chebyshev polynomials [16]. The second class of post-processing techniques include an approach that involves reconstruction of the AUT response based on a set of measurements performed in different locations of the non-anechoic test site [21]. The structure characteristics are then extracted based on a set of weighted averages of the performed measurements. Although the method is easy to implement, it is also characterized by relatively high measurement errors compared to other solutions in the literature [22]. In [22], a characterization of the non-anechoic environment is proposed. The approach involves measurement of the reference antenna (RA) which was previously determined in an anechoic environment, followed by extraction of the impulse response of the non-ideal test-site. The obtained data is then used for correction of the AUT measurements performed in the characterized non-ideal conditions. Unfortunately, the method of [22] has only been demonstrated based on EM simulations. It should be noted that the main assumption behind the approach is the static nature of the propagation environment which does not hold due to interferences from the external EM sources.

Regardless of the demonstrated usefulness, the cost-related benefits of post-processing approaches when applied to non-anechoic measurements seem to remain unnoticed in the available literature [22], [23]. For instance, in [24], [25], and [26], the measurements are performed in anechoic chambers which are not only expensive but also provide environments that do not pose much of a challenge for the correction methods. On the other hand, while validation of antenna performance at non-anechoic test sites has been explored [4], [12], [14], [15], the tests have been performed using expensive, laboratory-grade equipment (i.e., VNAs, radio-frequency cables, professional positioning heads, etc.). One might argue that the mentioned high-performance gear is not necessary for non-ideal measurements as the precision is counterbalanced by the low-quality of the noisy propagation environment. Having that in mind, the problem concerning low-cost characterization of far-field responses with reasonable accuracy remains open.

In this paper, an affordable system for measurements of antenna far-field performance figures in non-anechoic environments is considered. The setup comprises two, in-house developed, rotary heads that enable precise two-degree-of-freedom control of the RA-AUT angular position, a low-cost open-hardware VNA that can operate in a frequency range from 100 kHz to 6 GHz [27], as well as software for data acquisition and post-processing. Apart from the substitution of the laboratory-grade VNA with open-hardware-based solutions, the new aspects of the work include the introduction of the time-domain-based correction method for post-processed gain and the exploitation of multiple measurements for extraction of far-field responses. The performance of the system has been demonstrated using two antenna structures for which radiation patterns, and single-direction gain over frequency have been obtained. The results have been compared against the responses obtained in anechoic chamber. Additionally, the low-cost VNA has been validated against the laboratory grade device in terms of its accuracy. The average difference between the results obtained in the discussed setup compared to the controlled environment amounts to only –26 dB. With an overall construction cost of around 3630 USD, the considered system is two orders of magnitude cheaper than the laboratory-grade VNA. The details of the system are available in an online repository [38].

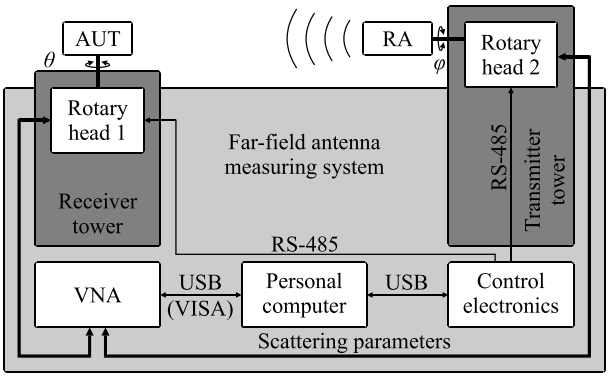

FIGURE 1. Open-hardware measurement system – a block diagram.

II. MEASUREMENT SYSTEM

Figure 1 shows a block diagram of the considered measurement system and its components, i.e., (i) an open-hardware VNA, (ii) in-house-fabricated rotary heads, and (iii) radio-frequency (RF) adapters and cables. The software that maintains the angular position of the heads, realizes the acquisition and post-processing of data is also an integral part of the setup. The heads have been designed in Autodesk Inventor, and machined from steel. Each head consists of rotary cores mounted on the base through a set of bearings. High angular resolution of rotation is ensured by a gear with 1:3.6 ratio driven by a 200-step motor. Heads are also equipped with a set of dedicated pins that enable their mating with a standard geodesy tribrach. The latter ones offer precise three-axis leveling capability and play the role of interfaces between heads and geodesy tripods. High-performance RF connectivity between the core and base of each head is realized using the SR1803 rotary joint from Fairview Microwave [28]. The angular position is controlled using a customized driver circuit based on an STM8 microcontroller. It is worth noting that the control electronics implement electrostatic discharge protection, as well as a communication interface based on a RS-485 standard [29], [30]. Both heads are enclosed in the in-house developed cases fabricated using the additive technology. Connection of the devices with a personal computer (PC) is maintained using a standard USB-to-RS-485 interface. Figure 2 shows a photograph of the manufactured head.

The measurements are carried out using Libre VNA, an affordable, USB-based, two-port vector network analyzer developed as an open-hardware project [27]. The device

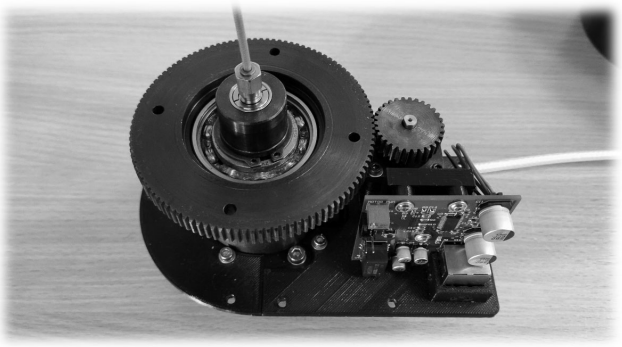

FIGURE 2. Head of the positioning system without enclosure.

realizes the functionality of an RF frontend capable of performing S-parameter measurements simultaneously in two ports over a frequency range of 100 kHz to 6 GHz. The rudimentary digital post-processing of the RF signals is realized using a field programmable gate array (FPGA), whereas further manipulation and post-processing of the signals is handled by the PC application. The latter supports, among others, the acquisition of up to 65,000 frequency points (in interval-based sweeps), time-domain functionality, four-port measurements in the scalar network analyzer configuration (through the realization of measurements using two units), as well as a variety of calibration methods along with support for automatic calibration. It is worth emphasizing that, on the functional level, the discussed VNA exceeds the capabilities of many professional devices. On the other hand, due to low-cost of the components used for the construction of the RF frontend it offers a noticeably lower dynamic range compared to many laboratory-grade devices. However, the parameter is maintained above the level of 60 dB over the (relatively narrow) frequency range which is considered sufficient for the experiments considered in this work.

RF interconnection of the VNA with the rotary heads is realized using the low-loss Sucoflex 126 coaxial cables with 3.5 mm connectors [31]. Direct mating between rotary joints and antennas is realized using the Minibend-16 assemblies which offer a short bending radius, high phase stability, and relatively low loss [31]. A standard PC is used to run software for the rotation of the heads, gathering (Python), and post-processing (MATLAB) of the data. The PC-to-VNA communication during the measurement process is realized over USB using the SCPI (standard commands for programmable instruments) interface [32].

III. MEASUREMENTS CORRECTION

The RA-AUT transmission obtained in non-anechoic conditions is corrected using a time-gating algorithm calibrated to the propagation conditions at the test site. The calibration process is automatic and involves optimization using a greedy heuristic algorithm. In this section, a concise discussion of TGM and site-calibration routine is provided. The considerations are followed by the description of the procedure oriented towards exploiting multiple measurements for the extraction of far-field characteristics, as well as the introduction of the gain-correction factor based on time-domain analysis of the impulse responses. More comprehensive explanations of the TGM-based concepts can be found in [4], [12], and [20].

A. TIME-GATING METHOD

The goal of the TGM algorithm is to perform the following a correction: $\boldsymbol{R} \rightarrow \boldsymbol{R}_c$, where $\boldsymbol{R} = \boldsymbol{R}(\boldsymbol{\omega}, \boldsymbol{\Phi})$ represents a $K \times P$ matrix of the RA-AUT transmission coefficients (i.e., S_{21}) where $\boldsymbol{\omega} = [\omega_1 \ldots \omega_K]^T$ denotes the sweep around the frequency of interest $f_0 = 0.5 \cdot (\omega_K + \omega_1)$ and $\boldsymbol{\Phi} = [\phi_1 \ldots \phi_P]^T$ is the vector of angular AUT positions w.r.t. RA. Note that f_0 denotes the frequency at which the far-field response of the antenna (e.g., radiation pattern) is to be obtained; $\boldsymbol{R}_c = \boldsymbol{R}_c(f_0, \boldsymbol{\Phi})$ is a vector that represents the corrected response of the AUT obtained at f_0 in a function of $\boldsymbol{\Phi}$ angles. It should be emphasized that $\boldsymbol{R}_c$ correction can also be used to extract single-direction antenna gain vs. M-point frequency sweep as $\boldsymbol{R}_{\mathrm{cg}}(\boldsymbol{f}, \phi) = [R_c(f_1, \phi_p) \ldots R_c(f_M, \phi_p)]^T$, where $\boldsymbol{f} = [f_1 \ldots f_M]^T$ and ϕ_p is the selected angular position of the RA-AUT system. In other words, the acquisition of data at multiple center frequencies involves a set of measurements with a constant angular position, yet as a function of $\boldsymbol{f}$.

For the given ϕ_p, the TGM is performed in the following steps [4], [12]:

1) Attenuate the frequency-domain response $\boldsymbol{R}(\boldsymbol{\omega}, \phi_p)$ at the edges of the sweep $\boldsymbol{\omega}$;
2) Convert the resulting frequency sweep to the N-point time-domain representation $\boldsymbol{T}(\boldsymbol{t}, \phi_p)$;
3) Apply a window function around the part of the time-domain signal that corresponds to LoS transmission;
4) Reset the impulse response to the frequency-domain and select the first K-points of the resulting N-element vector as the corrected response.

It should be noted that, although Step 1 is not mandatory, it improves the causality of the impulse response obtained from the measurement data [4], [12], [20]. The TGM correction is repeated for all desired angular locations of the RA-AUT system. Note that the correction algorithm performance highly depends on coefficients such as the frequency resolution $\partial\omega = \omega_2 - \omega_1$ (associated with the number of points K at which the frequency data has been obtained), but also the number of time-domain samples N, bandwidth around the center frequency of interest $B = \omega_K + \omega_1$ (which affects the resolution of the signal in the time-domain as $\partial t = B^{-1}$), as well as interval, location, and type of the utilized time-gating window [4], [12], [20]. Here, $K = 201$, $N = 2^{log2(\lceil K \rceil)+3}$, and $B \geq c \cdot (3 \cdot D)^{-1}$, where D is the antenna size and c is the speed of light, are derived from the recommendations of [4]. The parameters of the time-gating window (here, the Hann function) are identified using the calibration method outlined in the following section.

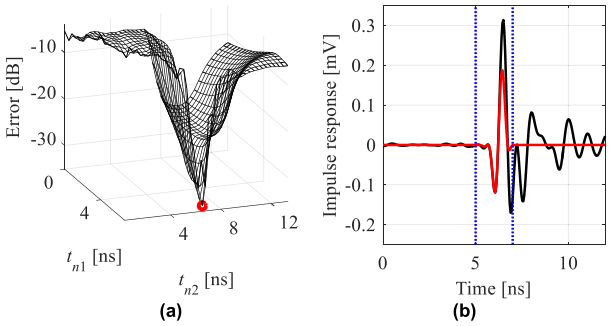

FIGURE 3. TGM: (a) discrepancy between the measurements performed in anechoic and non-anechoic conditions as a function of TGM intervals, as well as (b) impulse response of the antenna before (black) and after (red) correction using the TGM window applied for the selected interval (blue). Note that the difference in amplitudes of the reference and modified signals due to windowing is noticeable.

B. TEST SITE CALIBRATION ALGORITHM

The site calibration involves automatic tuning of the gating window interval in order to maximize the performance of the TGM. The algorithm is executed on the data acquired for a so-called calibration antenna (CA), i.e., the structure for which accurate measurements (i.e., obtained in the anechoic chamber, open-test site, or high-fidelity EM simulations) are available.

The goal of the calibration algorithm is to identify a possibly tight interval of the time-gating window around the part of the impulse response that corresponds to the LoS transmission within the RA-AUT system in order to reduce the contribution of EM noise to the measured AUT performance. The effects of adjusting the gating window on the performance of TGM correction, as well as the visualization of the impulse response before and after the filtering of interferences are illustrated in Fig. 3. It should be noted that the functional landscape that represents the discrepancy between CA measurements from non-anechoic and laboratory conditions represents a narrow valley with steep slopes. Consequently, appropriate adjustment of the window function is essential for high-quality post-processing of the far-field performance figures [4], [12].

The calibration process involves measurement of the CA in the non-anechoic test site, followed by optimization of intervals at a set of frequencies of interest $\boldsymbol{f}_0 = \{f_{0,\mathrm{j}}\}_j = 1 \ldots J$. Note that the intervals can be determined for $J = 1$. However, increasing the number of frequency points may mitigate the risk of setting an overly tight window adjustment resulting in the truncation of a fraction of the impulse response corresponding to LoS transmission [4]. At each frequency $f_{0,\mathrm{j}}$, the initial interval bounds are determined as $t_{j.1}^{(0)} = \min(\boldsymbol{t}_{\mathrm{pos},j})$ and $t_{j.2}^{(0)} = \min([\max(\boldsymbol{t}_{\mathrm{pos},j}), t_{\max,j}])$. Here, the components of $\boldsymbol{t}_{\mathrm{pos},j} = [t_1 \ldots t_P]^T$ are calculated from [4]:

$$t_p = \arg\max_{t_p \in \boldsymbol{t}} \left(|\boldsymbol{T}\left(\boldsymbol{t}, \phi_p\right)| \right) \tag{1}$$

Note that $t_{\max,j} = 2 \cdot M(\boldsymbol{t}_{\mathrm{pos},j}) - \min(\boldsymbol{t}_{\mathrm{pos},j})$—with $M(\cdot)$ being the median operation—is used to mitigate the risk of misinterpreting the EM interference as LoS for the angular positions of the AUT that correspond to, e.g., side-lobe radiation [4]. Clearly the latter is pertinent to directional antennas.

Upon identification of the initial interval, a greedy heuristic method is used to evaluate the quality of TGM correction at the set of perturbed designs $\boldsymbol{t}_{\mathrm{pert}}$ generated around the $t_{j.1}, t_{j.2}$ bounds. In each step i of the process, the correction performance associated with the interval from $\boldsymbol{t}_{\mathrm{pert}}$ is determined as follows [4]:

$$[t_{j.1}^{(i+1)} \; t_{j.2}^{(i+1)}] = \arg \min_{t_{j.1}, t_{j.2} \in \boldsymbol{t}_{\mathrm{pert}}^{(i)}} U\left(\boldsymbol{t}_{\mathrm{pert}}^{(i)}\right) \tag{2}$$

where U is a scalar objective function of the form [4]:

$$U = \left\| \boldsymbol{R}_{c.i}\left(f_{0,j}, \boldsymbol{\Phi}\right) - \boldsymbol{R}_r\left(f_{0,j}, \boldsymbol{\Phi}\right) \right\|_2 \tag{3}$$

Here, $\boldsymbol{R}_{c.i}$ is the refined, response of the CA obtained in non-anechoic conditions for $t_{j.1}$, $t_{j.2} \in \boldsymbol{t}_{\mathrm{pert}}^{(i)}$, at the $f_{0,\mathrm{j}}$ frequency and $\boldsymbol{R}_r$ denotes the reference response (e.g., obtained in the anechoic chamber, or from EM simulations). The parameters $t_{j.1}^{(i+1)}$, $t_{j.2}^{(i+1)}$ are used as the bounds for generation of the $\boldsymbol{t}_{\mathrm{pert}}^{(i+1)}$ set. The optimization is terminated when the correction performance is the same for two consecutive iterations. Otherwise, $i = i+1$ and the tuning process (2) is repeated. The optimized intervals are $t_{j.1}^{*} = t_{j.1}^{(i)}$ and $t_{j.2}^{*} = t_{j.2}^{(i)}$, respectively.

Upon execution of the algorithm at all frequency points, the final interval is determined as $t_1^{*} = \lfloor E(\{t_{j.1}^{*}\}_{j=1\ldots J}) \rfloor$ and $t_2^{*} = \lceil E(\{t_{j.2}^{*}\}_{j=1\ldots J}) \rceil$. Here, $\lfloor \cdot \rfloor$, $\lceil \cdot \rceil$, represent functions that round down, up to the nearest multiple of ∂t (cf. Section III. A), whereas $E(\cdot)$ is the averaging operator [4]. Once the calibration is performed, the obtained interval bounds are considered valid for the antennas characterized by comparable dimensions that are to be measured at the given non-anechoic test site. For a more comprehensive discussion on the discussed correction procedure see [4].

C. EXTERNAL EM NOISE REDUCTION

Due to the lack of test site shielding, the refined AUT responses are contaminated by the EM noise from external sources (blended with the impulse-response of the measured system, especially its part corresponding to LoS transmission) [4]. Here, effects of external EM signals on the responses are mitigated through re-construction of the far-field response using a set of measurements.

Let $\boldsymbol{R}_c^{(s)}$, $s = 1, \ldots, S$, be the sth far-field response of the AUT corrected using the TGM algorithm in the calibrated test site. The refined response can be extracted as a convex combination of the individual measurements:

$$\boldsymbol{R}_c^{*}\left(f_0, \boldsymbol{\Phi}\right) = \sum_{s=1}^{S} \alpha_s \boldsymbol{R}_c^{(s)}\left(f_0, \boldsymbol{\Phi}\right) \tag{4}$$

where the coefficients α_s are obtained from the time-domain-based auto-/cross-correlation of the uncorrected far-field

measurements $\boldsymbol{R}^{(s)} = \boldsymbol{R}^{(s)}(f_0, \boldsymbol{\Phi})$ obtained around the calibration frequencies:

$$\alpha_s = \frac{c_s}{\sum\left(\left[c_1 \cdots c_S\right]^{-1}\right)} \tag{5}$$

where

$$c_s = \max\left(cor\left(F^{-1}\left(\boldsymbol{R}^{(1)}\right), F^{-1}\left(\boldsymbol{R}^{(s)}\right)\right)\right) \tag{6}$$

Here, $cor(\cdot)$ and $F^{-1}(\cdot)$ denote the auto-/cross-correlation and the inverse fast Fourier transform, respectively. Note that the contribution of individual $\boldsymbol{R}_{c(s)}$ responses in (4) is determined based on the correlations of uncorrected measurements. The rationale behind the analysis of correlations is that increased contributions of far-field signals characterized by ''distinct'' impulse responses would allow to remove uncorrelated noise. It is worth noting that increasing S improves correction performance, yet at the expense of increased measurement time. Here, $S = 5$ to maintain an acceptable data gathering cost.

D. TGM-BASED GAIN REFINEMENT

The TGM implementation considered here attenuates the noise through the application of the Hann window centered around the fraction of the impulse response corresponding to the LoS of the RA-AUT system. Due to the bell-like shape of the window function, its application might lead to a reduction in the LoS amplitude compared to the one obtained without the post-processing. The problem has been conceptually illustrated in Fig. 3(b). Having in mind that the distance between the antennas affects attenuation of the S_{21} between them, the reduced amplitude of its corresponding impulse response has to be accounted for in gain estimation.

Let, $\boldsymbol{G}_c(\boldsymbol{f}, \phi_p) = (\boldsymbol{P}_l(\boldsymbol{f}) + \boldsymbol{R}_{cg}(\boldsymbol{f}, \phi_p))/2$ be the gain of the AUT over frequency sweep $\boldsymbol{f}$ obtained using the two-antenna method for the angular position ϕ_p [33], where $\boldsymbol{P}_l(\boldsymbol{f})$ and $\boldsymbol{R}_{cg}(\boldsymbol{f}, \phi_p)$ represent the power loss over the frequency sweep resulting from the Friss transmission model and the S_{21} over frequency sweep corrected using the algorithm of Section III. *A* (both expressed in dB) [34]. Here, the refined gain that accounts for the increased attenuation being a byproduct of TGM is given as:

$$\boldsymbol{G}_c^*\left(\boldsymbol{f}, \phi_p\right) = \boldsymbol{G}_c\left(\boldsymbol{f}, \phi_p\right) + \gamma\left(\boldsymbol{a}\right) \tag{7}$$

where $\gamma(\boldsymbol{a}) = (\sigma(\boldsymbol{a}) + E(\boldsymbol{a}))/2$ is the correction factor with $\sigma(\cdot)$ being a standard deviation and $\boldsymbol{a} = [a_1, \ldots, a_M]^T$ represents a vector of transmission amplitude change in the time domain. The coefficients of $\boldsymbol{a}$ are extracted as:

$$a_m = \max\left\{\left|\boldsymbol{T}_m\left(\boldsymbol{t}_j, \phi_p\right)\right|\right\} - \max\left\{\left|\boldsymbol{T}_m\left(\boldsymbol{t}_j, \phi_p\right) \circ \boldsymbol{W}\left(\boldsymbol{t}_j\right)\right|\right\} \tag{8}$$

Here, $\boldsymbol{T}_m(\boldsymbol{t}_j, \phi_p) = F^{-1}(\boldsymbol{R}(\omega_m, \phi_p))$ represents the impulse response obtained for the frequency sweep centered around mth frequency of interest (cf. Section III.*A*), whereas $\boldsymbol{t}_j$ and $\boldsymbol{W}(\boldsymbol{t}_j)$ denote the fraction of the impulse response determined by t_1^* and t_2^* instances and the Hann window defined in the mentioned interval; "$\circ$" is the component-wise multiplication. The gain correction factor of (7) is calculated over all $\boldsymbol{f}$ frequency points of interest. It should be noted that the contribution of (8) to the corrected gain depends on the type of window function used for TGM, as well as its location w.r.t. the fraction of the impulse response that corresponds to LoS between RA and AUT.

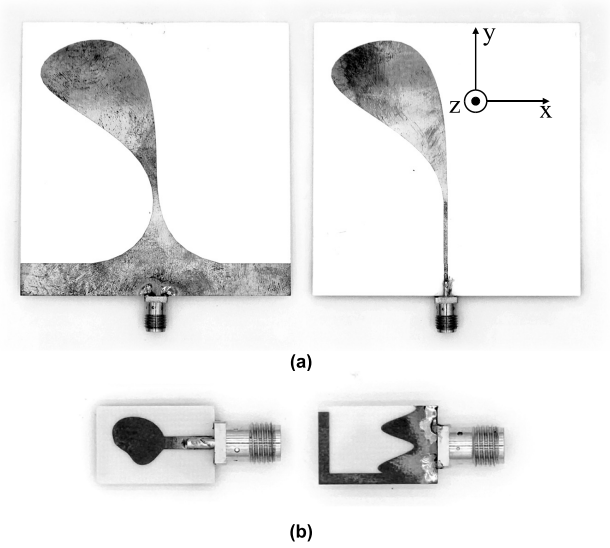

FIGURE 4. Photographs of the antennas considered for experiments (not in scale): (a) Vivaldi [35], and (b) monopole [36].

IV. RESULTS

In this section, the presented non-anechoic measurement system is demonstrated using an antipodal Vivaldi and a compact monopole antennas. Photographs of the radiators are shown in Fig. 4. The considered experiments include measurements of the radiation patterns (with 5° angular resolution) in the azimuth plane, as well as single-direction gain over frequency. The RA-AUT data have been obtained at a 5.5 × 4.5 × 3.1 m^3 test site. Besides the installation of the towers (cf. Section II), the room is not tailored to measurements of antenna far-field performance. Note that the line-of-sight RA-AUT distance is around 1.6 m, whereas the separation of AUT from the nearest perpendicular wall is 2.2 m. The VNA is calibrated and its output power is set to 0 dBm [27]. As already mentioned, the transmission between the antennas is recorded as S_{21} (which offers improved dynamic range w.r.t. S_{12} measurement for the considered device) [27]. Furthermore, the test site is packed with equipment that causes multi-path propagation of signals. The schematic view and photograph of the test site are shown in Fig. 5.

A. VIVALDI ANTENNA

The first case study considers measurements of the Vivaldi antenna of Fig. 4(a) which is used as both the RA and AUT [35]. The antenna size is roughly 10 cm, which corresponds to $B = 1$ GHz (see Section III-A.) [4].

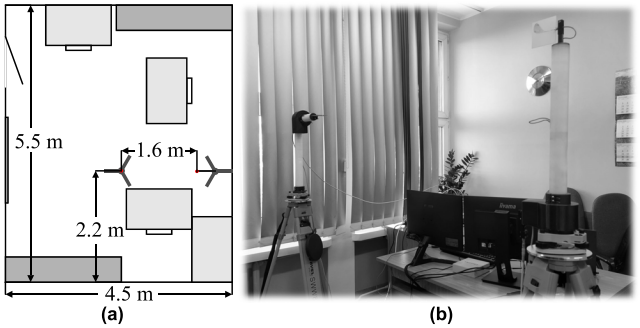

FIGURE 5. Test site for non-anechoic measurements: (a) schematic view and (b) photograph.

Measurements of the structure's performance are preceded with calibration of the TGM intervals using the method of Section III. *B*. Here, the process has been performed for the center frequency of 5 GHz. The reference data for calibration are the high-fidelity EM simulations of the radiator. The extracted bounds for the time-domain window are $t_1^* = 6$ ns, and $t_2^* = 8$ ns, respectively. In the next step, the transmission characteristics of the RA-AUT system (as a function of the angular location of the measured antenna) have been obtained around the 2.5 GHz, 4 GHz, and 5.5 GHz frequencies. For each f_0, the measurements have been repeated five times in order to execute the EM noise reduction of Section III. *C*. A comparison of the radiation patterns before and after TGM correction with the responses obtained in the anechoic chamber is shown in Fig. 6. The discrepancy between the patterns obtained before and after TGM-based correction—in terms of a root-mean square error (RMSE) averaged over all frequencies of interest—is only –23.8 dB. Consequently, the responses obtained as a result of the considered post-processing method are improved by almost 12 dB compared to uncorrected radiation patterns (average RMSE of –11.93 dB). It is worth noting that the RMSE-based discrepancy between the sequentially performed TGM-corrected measurements (variation from 0.1 dB to 0.2 dB) has been mitigated using the procedure of Section III. *C*.

The second experiment involves measurement of antenna gain in the yz-direction (see Fig. 4(a)) over the frequency span from 1.5 GHz to 5.5 GHz. It should be noted that, due to the acquisition of the RA-AUT transmission within the 1 GHz bandwidth around the frequency of interest, the maximum range for which gain can be obtained (without exceeding the operational bandwidth of the open-hardware VNA) is 5.5 GHz. The figure has been measured using the method of Section III. *D*. Note that, similarly as for the radiation patterns, the RA-AUT transmission has been acquired five times so as to combine the results (see Section III. *C*). A comparison of the responses obtained in the non-anechoic conditions before and after the correction is shown in Fig. 7. The results indicate that the presented approach substantially improves the accuracy of the gain compared to uncorrected measurements. At the same time, the correction factor (7) accounts for the amplitude attenuation due to the time-domain window. Overall, the discrepancy between the reference and the measured responses (averaged over the frequencies of interest) is only 0.12 dB, compared to 1.42 dB and 2.07 dB for uncorrected measurements and the responses obtained using TGM yet with no amplitude correction.

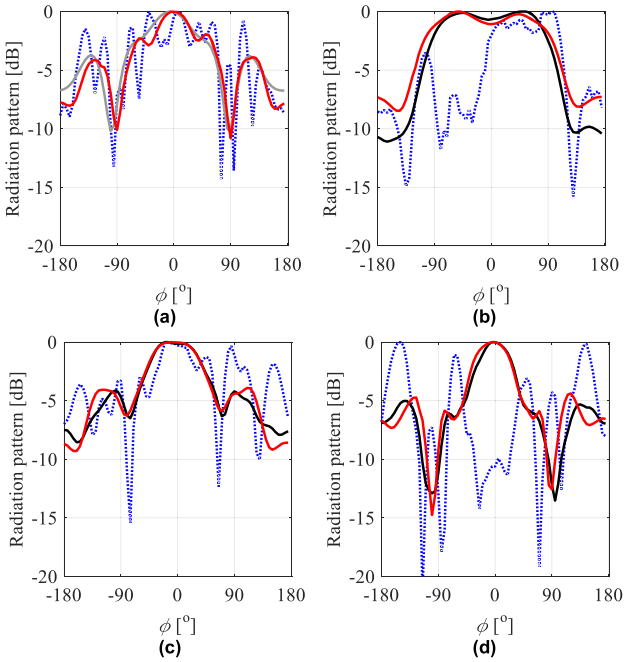

FIGURE 6. Vivaldi antenna – comparison of the radiation patterns before (blue) and after correction (red) with the EM-simulations (gray) and the anechoic chamber measurements at: (a) 5 GHz (calibration), (b) 2.5 GHz, (c) 4 GHz, and (d) 5.5 GHz frequency.

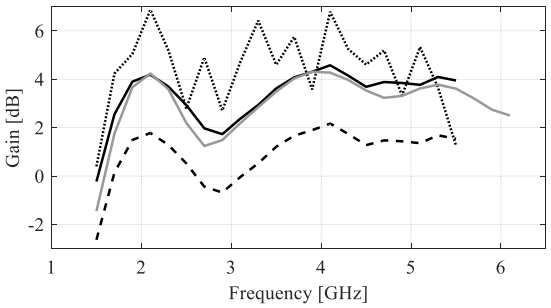

FIGURE 7. Vivaldi antenna – the reference (gray) vs. measured (black) gain (co-pol) obtained without correction (...), after TGM (– –), and as a result of TGM with amplitude correction (—).

B. COMPACT MONOPOLE ANTENNA

The second case study concerns measurements of the spline monopole of Fig. 4(b) [36]. Here, the Vivaldi antenna of Section IV-A is used as the reference structure. It should be noted that the monopole size is around 3 cm, which would necessitate setting the measurement to 3 GHz (cf. Section III. *A*). However, its lower frequency of operation is 3.1 GHz, which would limit the range of usable frequencies

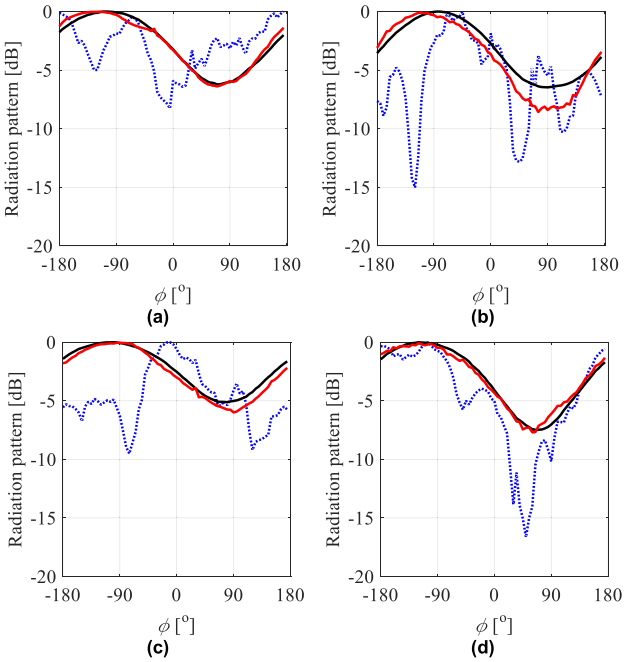

FIGURE 8. Compact monopole – comparison of the radiation patterns before (blue) and after correction (red) with the anechoic chamber responses at: (a) 5 GHz (calibration), (b) 3 GHz, (c) 4.5 GHz, and (d) 5.5 GHz frequency.

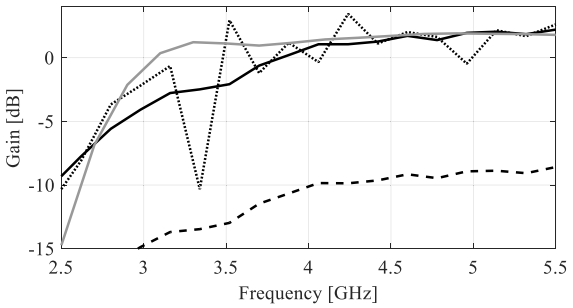

FIGURE 9. Monopole antenna – the reference (gray) vs. measured (black) gain (co-pol) obtained without correction (...), after TGM (– –), and as a result of TGM with amplitude correction (–·–).

to only around 1.5 GHz (from ∼3 GHz to 4.5 GHz, respectively). Consequently, the bandwidth has been set to $B = 2$ GHz as a trade-off between the VNA capabilities and the performance of the post-processing [4].

The test site calibration has been performed at 5 GHz frequency w.r.t. the anechoic chamber-based responses of the spline monopole (cf. Section III). The extracted time-gating interval bounds are $t_1^* = 5$ ns, and $t_2^* = 6.5$ ns, respectively. Upon calibration the antenna responses have been measured around 3 GHz, 4.5 GHz, and 5.5 GHz. Note that the bandwidth for the last frequency exceeds the capabilities of the VNA (cf. Section II). Here, the problem is mitigated by representing the transmission from 6 GHz to 6.5 GHz as the average of the responses acquired from 4.5 GHz to 6 GHz. The corrected radiation patterns shown in Fig. 8 indicate that the resemblance between the measurements from the test site

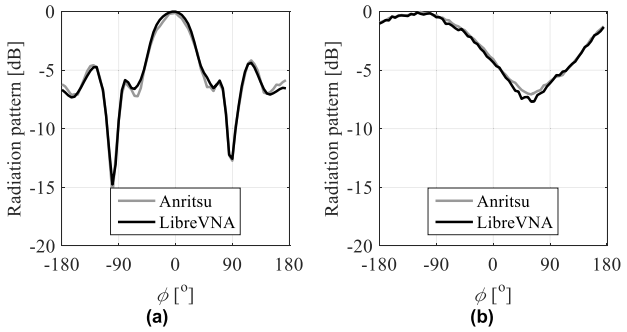

FIGURE 10. Comparison of far-field radiation patterns obtained in the considered test-site at 5.5 GHz frequency using Anritsu (grey) and LibreVNA (black) network analyzers for: (a) Vivaldi and (b) monopole antenna.

and the anechoic chamber is acceptable. Due to the small size of the considered monopole, as well as its relatively low gain accurate extraction of its far-field properties is more challenging compared to the Vivaldi structure. Overall, the average RMSE discrepancy between the reference and TGM-based results amounts to around –27.4 dB which represents around a 15 dB improvement compared to the uncorrected responses. Note that the RMSE-based discrepancy between the sequence of TGM-corrected measurements changes from 2.6 dB to 4.21 dB. Application of the procedure of Section III. *C* allows to mitigate the changes of the post-processed responses. Note that increased RMSE-based variation might result from both narrower bandwidth around f_0 (compared to the recommendation), but also small gain of the antenna.

The gain characteristics of the antenna measured over a frequency span of 2.5 GHz to 5.5 GHz in an yz-direction (see Fig. 4(b)) are shown in Fig. 9. The average discrepancy between the reference and corrected responses over the frequency band amounts to 0.78 dB, which is considered acceptable given the environmental conditions at the test site and the limited bandwidth around f_0. Note that neglecting the correction coefficient results in notable attenuation of the measured gain w.r.t. the reference responses (cf. Fig. 9).

V. COMPARISONS AND DISCUSSION

In this section, the quality of the measurements performed using the open-hardware VNA is compared against the results obtained using a laboratory-grade equipment manufactured by Anritsu [37]. A detailed cost-breakdown of the device and discussion of its features w.r.t. the existing far-field measurement systems are also provided.

A. PERFORMANCE

The test system has been compared in terms of the accuracy (w.r.t. the results obtained in the anechoic chamber) in configurations with: (i) the open-hardware VNA of Section II and (ii) the laboratory-grade network analyzer [37]. It should be emphasized that the measurement conditions for both considered test cases remain exactly the same (except for temporal changes of propagation conditions which remain beyond

TABLE 1. Non-anechoic test site: measurement performance using laboratory and open-hardware VNAs vs. anechoic chamber.

	Setup		Center frequency [GHz]				$\langle e_R \rangle$ [dB]
			2.5	4	5	5.5	
Vivaldi	(i)	e_R [dB]	–23.6	–21.3	–27.2	–23.3	–23.8
	(ii)	e_R [dB]	–22.9	–20.3	–26.5	–23.4	–23.4
	Setup		Center frequency [GHz]				$\langle e_R \rangle$ [dB]
			3	4.5	5	5.5	
Monopole	(i)	e_{Ra} [dB]	–29.8	–23.1	–28.3	–30.1	–28.0
	(ii)	e_R [dB]	–27.0	–21.6	–29.8	–31.6	–27.5

TABLE 2. Non-anechoic measurement system: cost breakdown.

Category	Item	Cost [USD]	Fraction of cost [%]
Heads	Steel and components	149	4.12
	Tools	52	1.44
Base	Tribrachs	113	3.12
	Tripods	258	7.12
Electronics	Components	160	4.42
	PCB manufacturing	24	0.66
	Rotary joints	489	13.5
RF connectivity	Cables	1420	39.1
	Connectors and adapters	235	6.52
Excitation	VNA	726	20.0
Total cost		3626	100.0

control). The results gathered in Table 1 indicate that, for the considered test cases and frequencies of interest, the average discrepancy between the measured performance (expressed in the form of the RMSE errors e_R) is below 0.5 dB. The discrepancies mostly result from the temporal dynamics of the measurement environment and the sequential nature of the data acquisition process [12]. A comparison of the radiation patterns obtained using both VNAs at 5.5 GHz frequency is shown in Fig. 10. As already indicated, the discrepancies between the characteristics obtained in the chamber and non-anechoic test-site can be considered acceptable for applications such as teaching, and/or low-budget research. However, the relatively low operational bandwidth of the open VNA limits the potential application scenarios of the antennas to be validated. For instance, the device is suitable only for experiments concerning the verification of the hardware dedicated to sub-6 GHz 5G communication, or related Internet of Things devices. On the other hand, the setup is suitable for structures compatible with WiFi systems characterized by broad practical applications.

B. COST AND COMPARISONS

A cost-breakdown of the discussed open-hardware system is provided in Table 2. It is worth noting that the components dedicated to maintaining RA-AUT position (i.e., heads, bases, and control electronics) correspond to only 21% of the overall cost, whereas the open-hardware VNA and connectivity gear amount to 20% and 59%, respectively. The high price of the RF cables is due to their low-loss and broad frequency range that exceed the requirements imposed by the VNA.

TABLE 3. Comparison of the presented system against existing solutions.

Setup	Metrics of interest*					
	(a)	(b)	(c)	(d)	(e)	(f)
(i)	+	+	–	+	+	+
(ii)	+	–/+	–	–/+	–/+	+
(iii)	–/+	–/+	–/+	–/+	–	–
This work	–	–	+	–/+	–	–

* The meaning of used symbols: + (high), –/+ (medium), – (low)

Having that in mind, the connectivity-related expenses could be further reduced (at least) by a factor of ten. Nonetheless, with the overall cost of around 3630 USD, the presented system is two orders of magnitude lower when compared just to the laboratory-grade VNA used for benchmark. It should be emphasized, however, that the latter offers substantially broader operational bandwidth (of up to 20 GHz). From the perspective of construction cost, the discussed system can be considered as an affordable solution with a range of applications where achieving the laboratory grade measurement precision is not of primary concern.

A comparison of the considered system with (i) anechoic chamber, (ii) open-test site, and (iii) commercial non-anechoic measurements setup (Geozondas, Lithuana) in terms of the metrics such as (a) cost, (b) frequency ranges, (c) mobility, (d) accuracy, (e) control over propagation conditions, or (f) the number of performance figures that can be measured ad-hoc is presented in Table 3. The results demonstrate that, owing to the use of open-source gear and lightweight positioning towers/heads, the considered device offers the lowest cost and highest mobility among considered solutions. At the same time, its operational bandwidth is limited, whereas accuracy of the extracted performance figures heavily relies on the quality (and setup) of the post-processing steps (cf. Section III).

VI. CONCLUSION

In this work, a low-cost system for characterization of antenna far-field performance in non-anechoic conditions has been discussed. The main components of the device are in-house developed positioning heads, a low-cost open-hardware VNA which operates in a range of up to 6 GHz, and the post-processing software that facilitates the extraction of the LoS signal from the non-anechoic measurements. The system capabilities w.r.t. the anechoic chamber have been demonstrated through measurements of two antenna structures. Furthermore, the performance of the utilized low-cost VNA has been compared against the laboratory-grade device. For the considered experiments the average discrepancy (expressed in terms of RMSA) between the results obtained using the open-hardware and professional equipment amounts to only –26 dB. Having in mind its low construction cost of only 3630 USD, the discussed system is suitable for budget constrained applications such as teaching, and low-frequency research. The details concerning the construction of the system are available through on-line repository.

Future work will focus on substitution of the machined rotary heads with the ones that can be fabricated using fused deposition modeling or stereolithography. It is expected that utilization of the additive manufacturing technologies will not only enable further reduction of the system cost but also increase its availability to institutions that lack advanced fabrication gear such as milling machines and/or lathes. Special care will be also dedicated to substitute the rotary joints with flexible cables, as well as the use of off-the-shelf components instead of the dedicated electronics. It is expected that the mentioned changes and advancements will contribute to further reduction of the system cost by at least a factor of two. As it comes to performance and applicability of the system, further improvement of post-processing will also be considered.

REFERENCES

[1] G. Kim and S. Kim, "Design and analysis of dual polarized broadband microstrip patch antenna for 5G mmWave antenna module on FR4 substrate," *IEEE Access*, vol. 9, pp. 64306–64316, 2021.
[2] J.-W. Kim, J.-I. Oh, S. H. Han, W.-Y. Song, S.-C. Chae, and J.-W. Yu, "Wideband circularly polarized antenna with reconfigurable 2-dimensional axial ratio beamwidth," *IEEE Access*, vol. 9, pp. 79927–79935, 2021.
[3] L. Hemming, *Electromagnetic Anechoic Chambers: A fundamental Design and Specification Guide*. Piscataway, NJ, USA: IEEE Press, 2002.
[4] A. Bekasiewicz, S. Koziel, and M. Czyz, "Time-gating method with automatic calibration for accurate measurements of electrically small antenna radiation patterns in non-anechoic environments," *Measurement*, vol. 208, Jan. 2023, Art. no. 112477.
[5] G. Evans, *Antenna Measurement Techniques*, Norwood, MA, USA: Artech House, 1990.
[6] K. Ballagh, "Calibration of an anechoic room," *J. Sound Vib.*, vol. 105, no. 2, pp. 233–241, 1986.
[7] S. Kurokawa, M. Hirose, and K. Komiyama, "Measurement and uncertainty analysis of free-space antenna factors of a log-periodic antenna using time-domain techniques," *IEEE Trans. Instr. Meas.*, vol. 58, no. 4, pp. 1120–1125, Apr. 2009.
[8] V. Molina-Lopez, M. Botello-Perez, and I. Garcia-Ruiz, "Validation of the open-area antenna calibration site at CENAM," *IEEE Trans. Instrum. Meas.*, vol. 58, no. 4, pp. 1126–1134, Apr. 2009.
[9] N. Munic, M. N. Stevanovic, A. Djordjevic, and A. Kovacevic, "Evaluation of radiating-source parameters by measurements in Faraday cages and sparse processing," *Measurement*, vol. 104, pp. 105–116, Jul. 2017.
[10] R. Gundersen, R. Norland, and C. R. Denby, "Geometric, environmental and hardware error sources of a ground-based interferometric real-aperture FMCW radar system," *Remote Sens.*, vol. 10, no. 12, 2018, p. 2070.
[11] C. Lucas, S. Leinss, Y. Bühler, A. Marino, and I. Hajnsek, "Multipath interferences in ground-based radar data: A case study," *Remote Sens.*, vol. 9, no. 12, art no. 1260, 2017.
[12] A. Soltane, G. Andrieu, E. Perrin, C. Decroze, and A. Reineix, "Antenna radiation pattern measurement in a reverberating enclosure using the time-gating technique," *IEEE Ant. Wireless Prop. Lett.*, vol. 19, no. 1, pp. 183–187, Dec. 2020.
[13] V. Fiumara, A. Fusco, G. Iadarola, V. Matta, and I. M. Pinto, "Free-space antenna pattern retrieval in nonideal reverberation chambers," *IEEE Trans. EM Comp.*, vol. 58, no. 3, pp. 673–677, Mar. 2016.
[14] P. Piasecki and J. Strycharz, "Measurement of an omnidirectional antenna pattern in an anechoic chamber and an office room with and without time domain signal processing," in *Proc. Signal Symp.*, Debe, Poland, 2015, pp. 1–4.
[15] G. L. Fernandez, S. Loredo, S. Zapatero, and F. L. H. Andres, "Radiation pattern retrieval in non-anechoic chambers using the matrix pencil algorithm," *Prog. Electromagn. Res. Lett.*, vol. 9, pp. 119–127, 2009.
[16] Z. Du, J. I. Moon, S.-S. Oh, J. Koh, and T. K. Sarkar, "Generation of free space radiation patterns from non-anechoic measurements using Chebyshev polynomials," *IEEE Trans. Antennas Propag.*, vol. 58, no. 8, pp. 2785–2790, Aug. 2010.
[17] D. A. Leatherwood and E. B. Joy, "Plane wave, pattern subtraction, range compensation," *IEEE Trans. Antennas Propag.*, vol. 49, no. 12, pp. 1843–1851, Dec. 2001.
[18] B. Fourestie and Z. Altman, "Gabor schemes for analyzing antenna measurements," *IEEE Trans. Antennas Propag.*, vol. 49, no. 9, pp. 1245–1253, Sep. 2001.
[19] E. N. Clouston, P. A. Langsford, and S. Evans, "Measurement of anechoic chamber reflections by time-domain techniques," *IEE Proc.*, vol. 135, no. 2, pp. 93–97, Apr. 1988.
[20] S. Loredo, M. R. Pino, F. Las-Heras, and T. K. Sarkar, "Echo identification and cancellation techniques for antenna measurement in non-anechoic test sites," *IEEE Antennas Propag. Mag.*, vol. 46, no. 1, pp. 100–107, Feb. 2004.
[21] S. M. Fróes, P. Corral, M. S. Novo, M. Aljaro, and A. C. C. Lima, "Antenna radiation pattern measurement in a nonanechoic chamber," *IEEE Ant. Wireless Prop. Lett.*, vol. 18, no. 2, pp. 383–386, Jan. 2019.
[22] J. Koh, A. De, T. K. Sarkar, H. Moon, W. Zhao, and M. Salazar-Palma, "Free space radiation pattern reconstruction from non-anechoic measurements using an impulse response of the environment," *IEEE Trans. Antennas Propag.*, vol. 60, no. 2, pp. 821–831, Feb. 2012.
[23] H. Moon, T. K. Sarkar, and W. Zhao, "Reconstruction of three-dimensional free space radiation pattern using non-anechoic measurements factored by the impulse response of the environment," in *Proc. IEEE Conf. Ant. Meas. App.*, Syracuse, NY, USA, 2016, pp. 1–4.
[24] M. Spirlet, C. Geuzaine, and V. Beauvois, "Experimental correction of radiation patterns between electromagnetic environments," *IEEE Trans. Ant. Prop.*, vol. 65, no. 3, pp. 1330–1338, Jan. 2017.
[25] G. Le Fur, "Improvement of antenna measurement results at low frequencies by using post-processing techniques," in *Proc. 8th Eur. Conf. Ant. Prop.*, Hague, Apr. 2014, pp. 1680–1684.
[26] J. Zhou, Z. Wang, C. Pang, Y. Li, and X. Wang, "Pattern reconstruction for polarimetric phased array antenna by efficient beam measurement," *IEEE Ant. Wireless Prop. Lett.*, vol. 20, no. 7, pp. 1312–1316, May 2021.
[27] (2021). *LibreVNA, An Open-Hardware Vector Network Analyzer*. [Online]. Available: https://github.com/jankae/LibreVNA
[28] *Rotary Joint SR1803*, Fairview Microwave, Lewisville, TX, USA.
[29] *Inventor*, Autodesk Inc., San Francisco, CA, USA, 2020.
[30] *STM8-Series Microcontroller*, STMicroelectronics, Geneve, Switzerland.
[31] *Microwave Cable Assemblies*, Huber+Suhner, Herisau, Switzerland.
[32] *SCPI*, IVI Foundation Corporate Office, Aaron Hall, Santa Rosa, CA, USA.
[33] K. K. Mistry, P. I. Lazaridis, Z. D. Zaharis, M. Akinsolu, B. Liu, and T. Loh, "Accurate antenna gain estimation using the two-antenna method," in *Proc. Ant. Prop. Conf.*, Birmingham, U.K., 2019, pp. 1–4.
[34] H. F. Harmuth and S. Ding-Rong, "Antennas for non-sinusiodal wave—Part I: Radiators," *IEEE Trans. Elec. Mag. Compat.*, vol. EMC-25, no. 1, no. 2, pp. 107–115, Feb. 1983.
[35] J. Bai, S. Shi, and D. W. Prather, "Modified compact antipodal Vivaldi antenna for 4–50-GHz UWB application," *IEEE Trans. Microw. Theory Techn.*, vol. 59, no. 4, pp. 1051–1057, Apr. 2011.
[36] A. Bekasiewicz, S. Koziel, P. Plotka, and K. Zwolski, "EM-driven multi-objective optimization of a generic monopole antenna by means of a nested trust-region algorithm," *App. Sci.*, vol. 11, no. 9, p. 3958, 2021.
[37] *MS2038C*, Anritsu Corp., Atsugi-shi, Japan.
[38] (2022). *An Open-Hardware Rotary Heads*. [Online]. Available: https://github.com/JanOlencki

JAN OLENCKI received the B.Sc. and M.Sc. degrees in electronic engineering from the Gdańsk University of Technology, Poland, in 2016 and 2020, respectively. He was an Analog and Mixed Signals Circuit Design Engineer with Synopsys Inc. During his graduate studies with the Gdańsk University of Technology, he was involved in the development of a low-cost setup for non-anechoic measurements of microwave antennas. He is currently with Antmicro Ltd., where he is responsible for the development of open-source software simulation frameworks.

VORYA WALADI received the B.S. degree in electronic engineering from the University of Science and Culture, Iran, in 2011, and the M.S. degree in telecommunication engineering, electromagnetic fields and waves from the Department of Electrical Engineering, IAU Science and Research Branch, Iran, in 2013. He is currently pursuing the Ph.D. degree with the Gdańsk University of Technology, Poland. His current research interests include antenna and wave propagation, signal processing, machine learning, and antenna measurement methods.

ADRIAN BEKASIEWICZ (Senior Member, IEEE) received the M.Sc., Ph.D., and D.Sc. (Higher Doctorate) degrees in electronic engineering from the Gdańsk University of Technology, Poland, in 2011, 2016, and 2020, respectively. He is currently an Associate Professor with the Gdańsk University of Technology. His research interests include the development of simulation-driven design and modeling methodologies, signal post-processing, multi-objective optimization, meta-heuristic algorithms, and inverse modeling methodologies with a focus on applications, such as the automatic development of microwave structures featuring unconventional topologies, miniaturization of microwave/RF components, in-door localization, as well as correction of real-world measurements and low-cost characterization of microwave/antenna components.

LEIFUR LEIFSSON received the bachelor's and master's degrees in mechanical engineering from the University of Iceland, Reykjavik, Iceland, in 1999 and 2000, respectively, and the Ph.D. degree in aerospace engineering from Virginia Tech, Blacksburg, VA, USA, in 2006. He is currently an Associate Professor of aerospace engineering with Purdue University, West Lafayette, IN, USA. His research interests include computational modeling, optimization, and uncertainty quantification of engineered systems with an emphasis on methods for multi-fidelity modeling and machine learning, aerodynamic shape optimization, aerodynamic flutter, model-based nondestructive evaluation, microwave devices, and food-energy-water nexus.